Inverse problems in computational ultrasound imaging and related applications

Adrian Basarab

Université de Toulouse, IRIT, Université Paul Sabatier Toulouse 3

IEEE IUS 2020, Las Vegas

Outline of the talk

Outline of the talk

The big picture

$$\mathbf{y} = T(\mathbf{x}) + \mathbf{n}$$

- $\mathbf{y} \in \mathbb{C}^M$ is the observed data
- $\mathbf{x} \in \mathbb{C}^N$ is the image of interest (not observed)
- $\mathbf{n} \in \mathbb{C}^M$ is the noise

T is the observation (forward) operator

- known : estimate $\mathbf{x}$ from $\mathbf{y}$
- unknown : estimate $\mathbf{x}$ and T from $\mathbf{y}$
  - Prior information on T (linear, parametric,...)

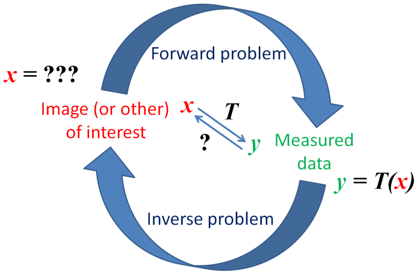

Examples of forward models in ultrasound imaging (non exhaustive)

Despeckling

- In the log-compressed envelope domain T is the identity operator

$$\mathbf{y} = \mathbf{x} + \mathbf{n}$$

- Example from Field II

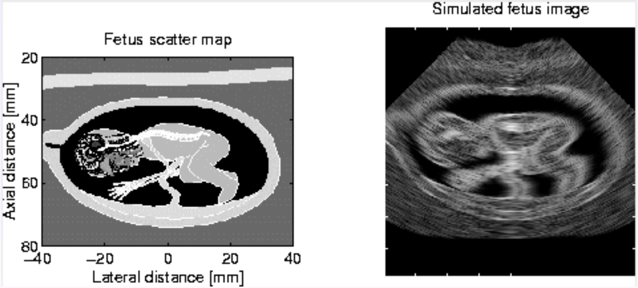

. A. Achim, A Bezerianos, P Tsakalides, Novel Bayesian multiscale method for speckle removal in medical ultrasound images, *IEEE TMI*, 2001.

Examples of forward models in ultrasound imaging (non exhaustive)

Compressed sensing

- T is a downsampling matrix in fast or/and slow time
- Applied to pre- or post-beamforming RF data
- Also used to decrease the number of active elements
- Φ is a fat random matrix

$$\mathbf{y} = \Phi\mathbf{x} + \mathbf{n}$$

3D line-wise sampling

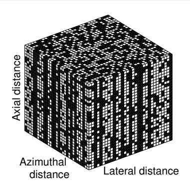

. P. van der Meulen, P. Kruizinga, J. G. Bosch, G. Leus, Coding Mask Design for Single Sensor Ultrasound Imaging, *IEEE TCI*, 2020.
. A. R, A. K. Thittai, Compressed Sensing Approach for Reducing Number of Receive Elements in Synthetic Transmit Aperture Imaging , *IEEE TUFFC*, 2020.
. M. Zhang *et al.*, Compressed Ultrasound Signal Reconstruction Using a Low-Rank and Joint-Sparse Representation Model, *IEEE TUFFC*, 2019.
. J. Liu, Q. He, J. Luo, A Compressed Sensing Strategy for Synthetic Transmit Aperture Ultrasound Imaging, *IEEE TMI*, 2017.
. Z. Chen, A. Basarab, D. Kouamé, A Compressive Deconvolution in Medical Ultrasound Imaging, *IEEE TMI*, 2016.
. O. Lorintiu *et al.*, A Compressed Sensing Reconstruction of 3D Ultrasound Data Using Dictionary Learning and Line-Wise Subsampling, *IEEE TMI*, 2015.
. G. David, J.-L. Robert, B. Zhang, and A. F. Laine, Time domain compressive beam forming of ultrasound signals, *J. Acoust. Soc. Am.*, 2015.
. A. Achim et al., Reconstruction of ultrasound RF echoes modelled as stable random variables, *IEEE TCI*, 2015.
. T. Chernyakova, Y. C. Eldar, Fourier-Domain Beamforming : The Path to Compressed Ultrasound Imaging, *IEEE TUFFC*, 2014.
. M. F. Schiffner, G. Schmitz, Fast pulse-echo ultrasound imaging employing compressive sensing, *IEEE IUS*, 2011.

Examples of forward models in ultrasound imaging (non exhaustive)

Deconvolution

- Linear image formation model, under the first order Born approximation
- In the RF domain, T is a convolution operator between the tissue refectivity function (x) and the PSF (h)

$$y = h \otimes x + n \Leftrightarrow \mathbf{y} = \mathbf{Hx} + \mathbf{n}$$

- Example - 3D printed phantom

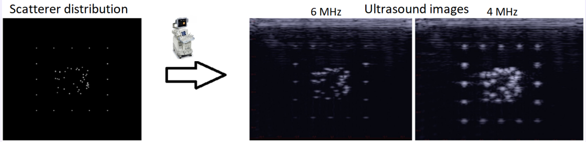

. A. Besson *et al.*, A Physical Model of Nonstationary Blur in Ultrasound Imaging, *IEEE TCI*, 2019.

. M. I. Florea, A. Basarab, D. Kouamé, S. A. Vorobyov, An Axially Variant Kernel Imaging Model Applied to Ultrasound Image Reconstruction, *IEEE SPL*, 2018.

. O. V. Michailovich, Non-stationary blind deconvolution of medical ultrasound scans, *SPIE Medical Imaging*, 2017.

. K. Hasan, S.-E. Rabbi, S. Y. Lee, Blind Deconvolution of Ultrasound Images Using l1 -Norm-Constrained Block-Based Damped Variable Step-Size Multichannel LMS Algorithm, *IEEE TUFFC*, 2016.

. N. Zhao, A. Basarab, D. Kouamé, J.-Y. Tourneret, Joint deconvolution and segmentation of ultrasound images using a hierarchical Bayesian model based on generalized Gaussian priors, *IEEE TIP*, 2016.

Examples of forward models in ultrasound imaging (non exhaustive)

Beamforming

- T relates the raw RF data to the image to be beamformed
- Depends on the acquisition geometry
- Can include the PSF

Other applications

- Tissue motion, blood flow, segmentation, tissue characterization, sparse array design, acoustic microscopy, ultrasound tomography, etc.

Plane-wave imaging

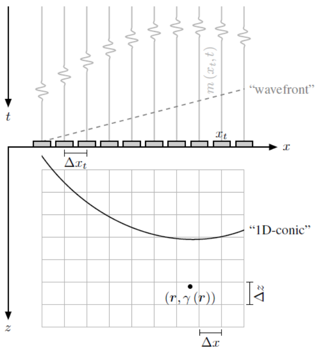

. A. Besson *et al.*, Ultrafast ultrasound imaging as an inverse problem : Matrix-free sparse image reconstruction, *IEEE TUFFC*, 2017.
. D. Bujoreanu, B. Nicolas, D. Friboulet, H. Liebgott, Inverse problem approaches for coded high frame rate ultrasound imaging, *Asilomar*, 2017.
. E. Ozkan, V. Vishnevsky, O. Goksel, Inverse problem of ultrasound beamforming with sparsity constraints and regularization, *IEEE TUFFC*, 2017.
. T. Szasz, A. Basarab, D. Kouamé, Beamforming through regularized inverse problems in ultrasound medical imaging, *IEEE TUFFC*, 2016.

Why inverting these models is a difficult problem ?

The solution is not unique and T is not invertible

- *Despeckling* : infinite number of ways to decompose an ultrasound image (**y**) into the sum between a despeckled image (**n**) and speckle noise (**n**)
- *Beamforming* : each different method will provide a different beamformed image from exactly the same acquired raw data
- *Compressed sensing* : in $\mathbf{y} = \Phi\mathbf{x} + \mathbf{n}$, Φ is a fat matrix, less measurements than unknowns
- *Deconvolution* : the PSF is a band-pass filter, thus canceling or strongly attenuating certain frequencies
- ...

Outline of the talk

Inversion and regularization

How to chose one (the !) solution from all the possible solutions ?

- Constrain the solution considering penalties
- Need for *a priori* information on $\mathbf{x}$ (regularization)
- Sparse regularization (considered here for illustration purpose)
  - The target image contains only a reduced number of non-zero pixels

MAP estimator

- Consider the image of interest is a random variable

$$\hat{\mathbf{x}} = \arg\max_{\mathbf{x}} p(\mathbf{x}|\mathbf{y}) = \arg\min_{\mathbf{x}} (-\log(p_y(\mathbf{y}|\mathbf{x})) - \log(p_x(\mathbf{x})))$$

- Note that DAS beamformer does not follow this trend, but it is a ML estimator ($\mathbf{x}$ is supposed deterministic, hypothesis of uncorrelated Gaussian noise)

. T. Chernyakova, D. Cohen, M. Shoham, Y. C. Eldar, iMAP Beamforming for High-Quality High Frame Rate Imaging, *IEEE TUFFC*, 2019.

Distributions promoting sparsity

$$\hat{\mathbf{x}} = \arg\max_{\mathbf{x}} p(\mathbf{x}|\mathbf{y}) = \arg\min_{\mathbf{x}} (-\log(p_y(\mathbf{y}|\mathbf{x})) - \log(p_x(\mathbf{x})))$$

Most common choice

- Under the assumption of additive Gaussian noise
- Laplace distribution to promote the sparsity of $\mathbf{x}$

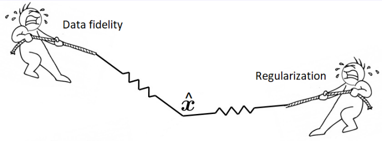

$$\hat{\mathbf{x}} = \arg\min_{\mathbf{x}} \|\mathbf{y} - T(\mathbf{x})\|_2^2 + \lambda \|\mathbf{x}\|_1$$

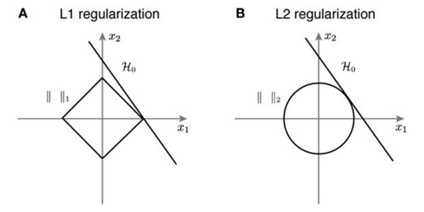

Outline of the talk

Interest of MR-US image fusion in endometriosis diagnosis

Joint work with O. El Mansouri, F. Vidal, D. Kouamé and J.-Y. Tourneret

- Presence of endometrial glands or stroma in sites different from the uterine cavity
- Typically affects women in their reproductive age and is associated with chronic pelvic pain and infertility
- Surgery is the standard treatment

Complementary medical imaging modalities

- MRI offers a large field of view but with limited spatial resolution
- High-frequency (10 MHz) ultrasound offers a good spatial resolution but with limited field of view and poor SNR

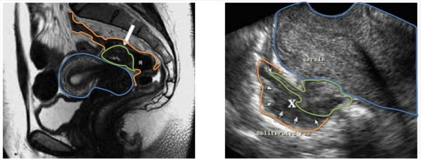

Uterus, deeply infiltrating endometriosis lesion, bowel wall

Outline of the talk

Forward models (1/2)

MRI (low spatial resolution and sampling, Gaussian noise)

$$\mathbf{y}_{\mathrm{m}} = \mathbf{SHx}_{\mathrm{m}} + \mathbf{n}_{\mathrm{m}}$$

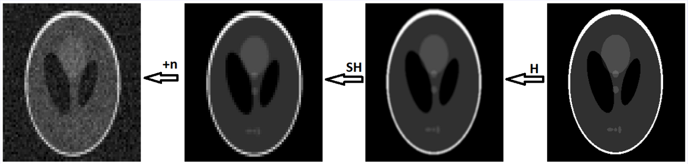

Ultrasound (Rayleigh noise)

$$\mathbf{y}_{\mathrm{u}} = \mathbf{x}_{\mathrm{u}} + \mathbf{n}_{\mathrm{u}}$$

- Super-resolution methods to estimate $\mathbf{x}_{\mathrm{m}}$
- Despeckling methods to estimate $\mathbf{x}_{\mathrm{u}}$
- **Fusion** : estimate an image $\mathbf{x}$ that gathers information from both $\mathbf{x}_{\mathrm{m}}$ and $\mathbf{x}_{\mathrm{u}}$

Forward models (2/2)

Different physical phenomena behind image acquisition

- $\mathbf{x}_{\mathrm{m}}$ and $\mathbf{x}_{\mathrm{u}}$ are different
  - Geometric misalignment modeled by a geometric transform T
  - No one to one correspondence between the gray levels

$$x_{\boldsymbol{u},i} = f_{\boldsymbol{c}}(T, \boldsymbol{x}_{\mathrm{m}}, \boldsymbol{u}) = \sum_{p+q \leq d} c_{pq} T(x_{\mathrm{m},i}^{p})(\nabla T(\boldsymbol{x}_{\mathrm{m}})^{H} \boldsymbol{u})_{i}^{q}$$

Finally

$$\boldsymbol{y}_{\mathrm{m}} = \boldsymbol{HSx} + \boldsymbol{n}_{\mathrm{m}}$$

$$\boldsymbol{y}_{\mathrm{u}} = f_{\boldsymbol{c}}(T(\boldsymbol{x}), \nabla T(\boldsymbol{x})^{H} \boldsymbol{u}) + \boldsymbol{n}_{\mathrm{u}}$$

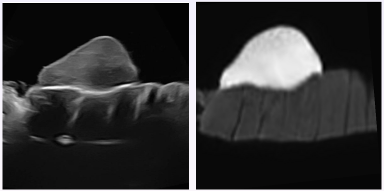

. A. Roche *et al.*, Rigid registration of 3D ultrasound with MR images : a new approach combining intensity and gradient information, *IEEE Trans. Med. Imaging*, 2001.
. O. El Mansouri, F. Vidal, A. Basarab, P. Payoux, D. Kouamé, J.-Y. Tourneret, Fusion of Magnetic Resonance and Ultrasound Images for Endometriosis Detection, *IEEE TIP*, 2020.
. O. El Mansouri, A. Basarab, M. Figueiredo, D. Kouamé, J.-Y. Tourneret, Ultrasound and magnetic resonance image fusion using a patch-wise polynomial model, *IEEE ICIP*, 2020.

Inverse problem

A priori information

- Gaussian noise in MRI and log-Rayleigh distributed speckle
- The fused image is piecewise smooth, *i.e.*, its gradient is sparse (total variation)
- The geometric transform is composed by a global affine transform and a local B-spline elastic deformation

$$(\hat{\boldsymbol{x}}, \hat{T}, \hat{\boldsymbol{c}}) = \underset{\boldsymbol{x}, T, \boldsymbol{c}}{\operatorname{argmin}} \quad \underbrace{\frac{1}{2}\|\boldsymbol{y}_{\mathrm{m}} - \boldsymbol{S}\boldsymbol{H}\boldsymbol{x}\|^2}_{\text{MRI data fidelity}}$$

$$+ \underbrace{\tau_1 \sum_{i=1}^{N} \exp\left[y_{\mathrm{u},i} - f_{\boldsymbol{c},i}(T, \boldsymbol{x}, \boldsymbol{u}) - \gamma(y_{\mathrm{u},i} - f_{\boldsymbol{c},i}(T, \boldsymbol{x}, \boldsymbol{u}))\right]}_{\text{US data fidelity}}$$

$$+ \underbrace{\tau_2\|\nabla \boldsymbol{x}\|^2 + \tau_3\|\nabla f_{\boldsymbol{c}}(T, \boldsymbol{x}, \boldsymbol{u})\|^2 + \tau_4 R_{\mathrm{s}}(T)}_{\text{regularization}}$$

. Matlab code available at https ://www.irit.fr/ Adrian.Basarab/codes.html

Outline of the talk

Fusion result on phantom data (1/2)

Homemade phantom mimicking pelvic anatomy

3D represenation

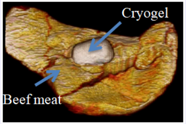

MRI on phantom

US on phantom

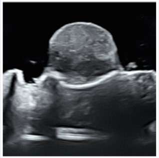

In vivo data

MRI *in vivo*

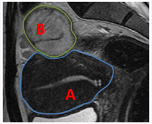

Endometrioma

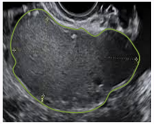

Uterus

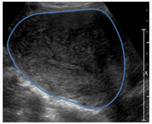

. F. Vidal, O. El Mansouri, D. Kouamé, A. Basarab, On the design of a pelvic phantom for magnetic resonance and ultrasound image fusion, *IEEE IUS*, 2019.

Fusion result on phantom data (2/2)

MRI

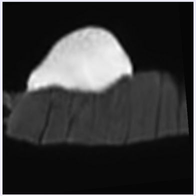

Ultrasound

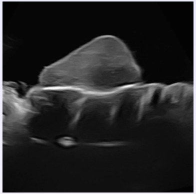

Fusion

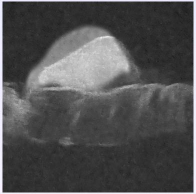

Fusion/Registration

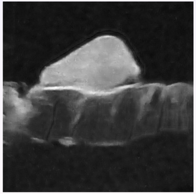

Deformation field

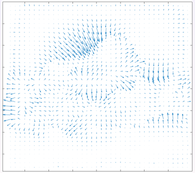

Outline of the talk

Lung ultrasound

Joint work with O. Karakus, N. Anantrasirichai, A. Aguersif, S. Silva, A. Achim

- Lung ultrasound (LUS) can help in assessing the fluid status of patients in intensive care
- LUS can be conducted rapidly and repeatably at the bedside, can reduce the need for CT scans (shorter delays, lower irradiation levels and cost)
- The common feature in all clinical conditions is the presence in LUS of a variety of line artefacts (e.g., pleural A, B-lines).

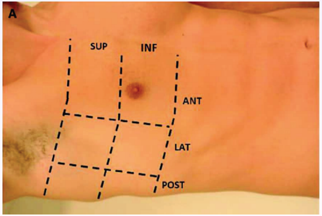

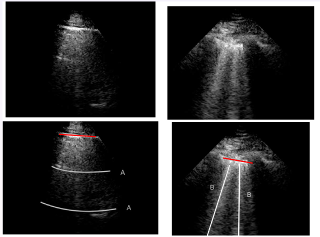

Outline of the talk

Forward model (1/2)

- The objective is to detect automatically lines in LUS (manual detection is time consuming : hundreds of images per patient, "random" line occurrence)
- Forward model based on Radon transform

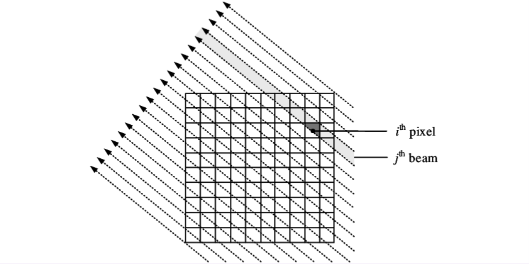

$$X(r,\theta) = \int_{\mathbb{R}^2} Y(i,j)\delta(r - i\cos\theta - j\sin\theta)\,didj$$

. N. Anantrasirichai, W. Hayes, M. Allinovi, D. Bull, and A. Achim, Line detection as an inverse problem : application to lung ultrasound imaging, *IEEE TMI*, 2017.

Forward model (2/2)

- Radon transform of a LUS image
- Speckle noise generates multiple false peaks resulting from collinear noisy edge points

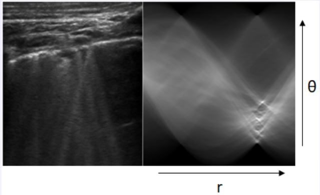

- Proposed solution : exploit the fact that only a **small number of lines** are to be detected

$$Y = \mathcal{C}X + N$$

- Y is the LUS image
- C is the inverse Radon transform
- X **is supposed sparse** and N an additive Gaussian noise

Inverse problem

- Cauchy distribution used to promote the sparsity of X

$$p(x) \propto \frac{\gamma}{\gamma^2 + x^2}$$

- MAP estimator

$$\hat{X}_{\text{Cauchy}} = \arg\min_X \frac{\|Y - \mathcal{C}X\|_2^2}{2\sigma^2} - \sum_{i,j} \log\left(\frac{\gamma}{\gamma^2 + X_{ij}^2}\right)$$

. O. Karakus, P. Mayo, A. Achim, Convergence guarantees for non-convex optimisation with Cauchy-based penalties, *arXiv preprint*.

. O. Karakus, N. Anantrasirichai, A. Aguersif, S. Silva, A. Basarab, and A. Achim, Detection of Line Artefacts in Lung Ultrasound Images of COVID-19 Patients via Non-Convex Regularization, *IEEE TUFFC special issue on Ultrasound in COVID-19 and Lung Diagnostics*, 2020.

. Matlab code available at https ://data.bris.ac.uk/data/dataset/z47pfkwqivfj2d0qhyq7v3u1i

Outline of the talk

Results

- Evaluation on nine COVID-19 patients

Original images

Ground truth

Proposed method

[Anantrasirichai *et al*, IEEE TMI'17]

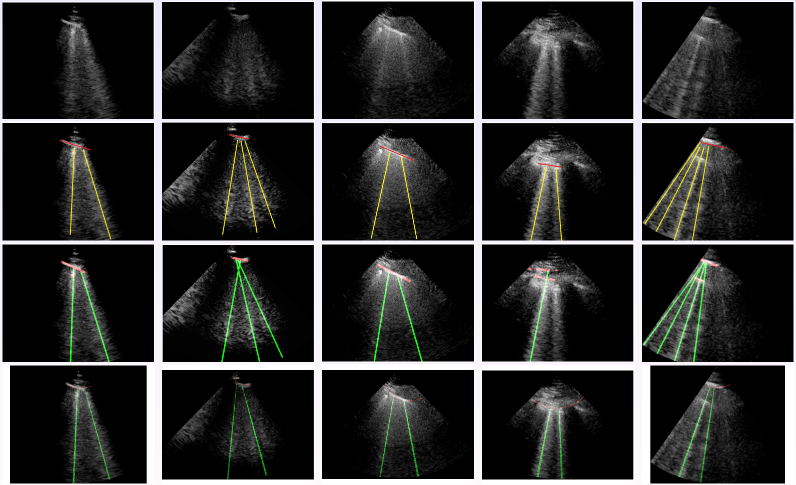

Results

- Evaluation on nine COVID-19 patients

Performance Metric	The Proposed Method	Anantrasirichai et al., IEEE TMI 2017
% Detection Accuracy	87.349%	78.916%
% Missed Detection	5.422%	13.855%
% False Detection	7.229%	7.229%
Specificity	7.692%	14.286%
Recall	94.118%	84.868%
Precision	92.308%	91.489%
F_1 Index	0.932	0.881
F_2 Index	0.938	0.861
$F_{0.5}$ Index	0.927	0.901
LR+	1.020	0.990
Area under curve (AUC)	0.963	0.931
The average number of B-lines (Ground Truth) = 1.520		
Average Detected B-lines	1.550	1.410
NMSE of number of detected B-lines	0.151	0.243

Results

- Evaluation on nine COVID-19 patients

Performance Metric	The Proposed Method	Anantrasirichai et al., IEEE TMI 2017
% Detection Accuracy	87.349%	78.916%
% Missed Detection	5.422%	13.855%
% False Detection	7.229%	7.229%
Specificity	7.692%	14.286%
Recall	94.118%	84.868%
Precision	92.308%	91.489%
F_1 Index	0.932	0.881
F_2 Index	0.938	0.861
$F_{0.5}$ Index	0.927	0.901
LR+	1.020	0.990
Area under curve (AUC)	0.963	0.931
The average number of B-lines (Ground Truth) = 1.520		
Average Detected B-lines	1.550	1.410
NMSE of number of detected B-lines	0.151	0.243

Conclusions (1/2)

Computational ultrasound imaging

- In most applications data is not sufficient (noise, incomplete data)
- Computational methods are used to avoid the ill-posedness of the resulting inverse problem

Model-based approaches

- Models include knowledge about the physics : fidelity, tractability
- Regularization terms are required and usually use fixed transforms or learned dictionaries (sparsity)
- Robust methods to outliers (model or regularizer not valid)

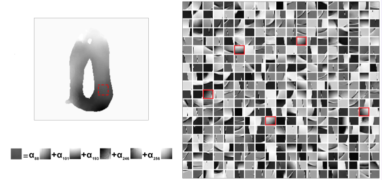

. N. Ouzir, A. Basarab, O. Lairez, J.-Y. Tourneret, Robust Optical Flow Estimation in Cardiac Ultrasound images Using a Sparse Representation, *IEEE TMI*, 2019.

. N. Ouzir, A. Basarab, H. Liebgott, B. Harbaoui, J.-Y. Tourneret, Cardiac motion estimation in ultrasound images using spatial and sparse regularizations, *IEEE TIP*, 2018.

Conclusions (2/2)

Machine (deep) learning

- More flexibility, but usually requires learning databases
- Useful for approaching complicated physical models
- Example in quantitative acoustic microscopy : *predict 500-MHz quantitative images from 250-MHz acquisitions*

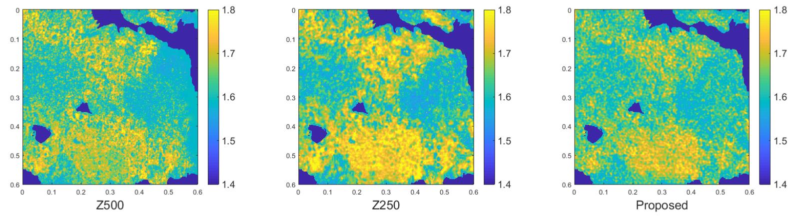

- Can also be used as (plug&play) regularizer combined with explicit physics-inspired models

. J. Mamou, T. Pellegrini, D. Kouamé, A. Basarab, A convolutional neural network for 250-MHz quantitative acoustic-microscopy resolution enhancement, *IEEE EMBC*, 2019.

Inverse problems in computational ultrasound imaging and related applications

Adrian Basarab

Université de Toulouse, IRIT, Université Paul Sabatier Toulouse 3

IEEE IUS 2020, Las Vegas